

VALIDATION STUDIES ON NUMERICAL PREDICTION OF SHIP SQUAT AND RESISTANCE IN SHALLOW WATER

P Mucha, University of Duisburg-Essen, Federal Waterways Engineering and Research Institute (BAW), Germany
G Deng, École Centrale de Nantes (ECN), France
T Gourlay, Curtin University, Australia
O el Mohtar, University of Duisburg-Essen, Germany

SUMMARY

A validation study on numerical prediction of ship squat and resistance in shallow water is presented. Two methods based on the solution of the Reynolds-averaged Navier-Stokes (RANS) equations, a Rankine Panel Method and a method based on slender-body shallow water theory were applied and explored in terms of reliability and performance. Validation studies relied on comparison with model experiments for Post-Panmax container ship Duisburg Test Case (DTC), Panmax Kriso Container Ship (KCS) and Kriso Very Large Crude Carrier (KVLCC) 2. It was found that all methods are generally capable of predicting midship sinkage with good accuracy, while the boundary element methods (BEM) yield larger deviations in higher Froude depth number regimes, especially in predicting trim. For very shallow water ship flows, resistance predictions with viscous flow solvers were shown to be sensitive to turbulence modelling, near-wall treatment and the boundary condition on the tank bottom. In shallow water lifting ship flows, consideration of squat was found to be crucial for accurate computation of transverse forces and yaw moments.

NOMENCLATURE

B_{WL}	Waterline breadth (m)
C_B	Block coefficient (-)
F_{nh}	Froude depth number (-)
g	Gravitational acceleration constant (m/s ²)
G	Rankine source
h	Water depth (m)
L_{pp}	Ship length between perpendiculars (m)
m	Ship mass (m)
\mathbf{n}	Face normal vector (-)
N	Hydrodynamic yaw moment (Nm)
q	Source strength
Re	Reynolds number (-)
R_T	Total ship resistance (N)
S	Control volume surface area (m ²)
$S(x)$	Sectional area (m ²)
S_w	Wetted surface area (m ²)
t	Time (s)
\mathbf{T}	Stress tensor (N/m ²)
T	Ship draft (m)
U	Ship speed (m/s)
u^*	Nondimensional wall velocity (-)
\mathbf{v}	Velocity vector (m/s)
V	Volume (m ³)
x	Longitudinal ship coordinate (m)
x_G	Longitudinal center of gravity (m)
X	Longitudinal hydrodynamic force (N)
y	Transverse ship coordinate (m)
y^+	Nondimensional wall distance (-)
y_g	Transverse center of gravity (m)
Y	Transverse hydrodynamic force (N)
z	Sinkage (mm)
β	Drift angle (°)
ζ	Free-surface elevation (m)
ϑ	Trim (1/60°)
λ	Scale factor (-)

ν	Kinematic viscosity (m ² /s)
ρ	Density of water (kg/m ³)
ξ	Relative distance of sources (m)
ϕ	Velocity potential (m ² /s)

1 DEFINITIONS

Under-keel clearance (UKC) is the distance from the ship keel at T to the vertical flow restriction at water depth h , valid for a Cartesian coordinate system located at the calm water level (Figure 1). Here, ship squat is defined as the decrease of UKC in response to pressure variations along the ship hull underway, which cause the ship to adjust her dynamic floating position in terms of a vertical translation (sinkage) and a rotational displacement in pitch mode of motion (trim), accompanied by a change of the ambient free-surface water level. Sinkage z is given positive downwards and trim ϑ positive aft-down in arc minutes [1/60°]. In straight ahead motion, ship Resistance R_T equals the negative longitudinal hydrodynamic force X .

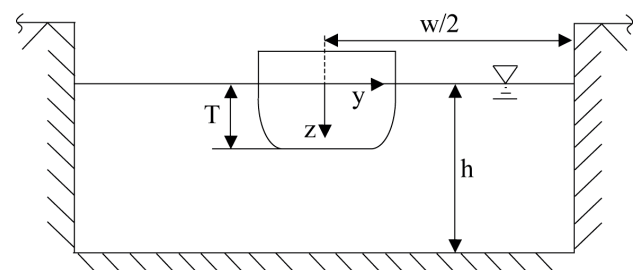


Figure 1. Coordinate systems and definitions for squat predictions in shallow water tanks

2 INTRODUCTION

The prediction of ship squat in shallow water has become an issue of renewed relevance for the hydrodynamic community, as port and waterway administrations face the challenge of growing ship sizes and request ship motion predictions to adapt accessibility to ports and waterways, or to regulate ship operation. Knowledge of shallow water induced added hydrodynamic forces is relevant for maneuvering and minimum power requirement prediction, especially in light of a more strict regulatory framework regarding environmental protection. Over the past three decades, numerical methods based on potential flow theory have been established as efficient tools for ship hydrodynamic analyses, including the application to squat prediction. Yet, the advance of numerical methods based on the solution of the Navier-Stokes equations - benefitted by a substantial increase in computational power - has enabled extended insight into shallow water ship flows. There are theoretical and experimental grounds to anticipate that the effects of turbulence and viscosity in such flow regimes are more dominant than in deep water, challenging the application of inviscid methods. This conflict is aggravated by the predominate investigation of model ship flows to establish a common basis for validation through comparison with experiments, because viscous effects are overbooked in lower Reynolds number regimes. For the particular problem of squat prediction the significance of these aspects was confirmed in the PreSquat workshop [1]. PreSquat aimed at benchmarking capabilities of available numerical methods for squat prediction through comparison with model experiments with the DTC container ship. With additional test cases added, this work drew upon the main findings of the workshop. Special attention was referred to the challenges involved in RANS-based predictions, addressing turbulence modelling, near-wall and free-surface treatment and consideration of rigid body motions.

3 CANDIDATE SHIPS AND TEST CASES

Main particulars of the candidate ships DTC, KCS and KVLCC2 are given in Table 1. No-full scale representations of these ships exist. They have been designed for the particular purpose of experimental hydrodynamic analyses and generation of benchmark data for comparison with numerical methods. Figure 2 presents lines plans (not drawn to scale). Geometries are publicly available online [2], [3].

3.1 MODEL EXPERIMENTS

Model experiments were performed in the shallow water tanks of the Development Centre for Ship Technology and Transport Systems (DST) in Duisburg, Germany, and the Bulgarian Ship Hydrodynamic Center (BSHC) in Varna, Bulgaria. Both facilities operate their tanks with

actual desired water depths and do not need to install so-called *false bottoms*.

3.1 (a) DTC and KCS

Towed model tests with DTC, appended with a rudder, were carried out at DST for the PreSquat workshop at $h/T=1.143$. Captive maneuvering tests in shallow water with KCS in bare hull condition were carried out at DST in the framework of research project [4]. Both models were tested at scale 40 at various water depths. KCS was investigated in different setups at $h/T=1.2$ and $h/T=1.3$ at four different forward speeds in the range of Froude depth numbers $F_{nh} = U/\sqrt{gh}$ from 0.27 to 0.68. The models were free to sink and trim, but otherwise constrained. Sinkage was measured by means of laser plates at positions ahead and behind amidships at $L_{pp}/2$. Static trim of the models was zero. DST's towing tank is 200m long and 10m wide. In both experimental setups the towing force point of attack was chosen as to ensure that no additional trim moment was induced. Vertical centers of gravity lay sufficiently below the waterline.

3.1 (b) KVLCC2

Captive maneuvering tests in shallow water were performed with a scale model ($\lambda=45.714$) of KVLCC2 at BSHC at $h/T=1.2$ in the framework of the SIMMAN workshop. Trim and sinkage were measured with wired potentio-meters attached to the model at positions ahead and behind amidships at $L_{pp}/2$. Static trim was zero. BSHC's towing tank is 200m long and 16m wide.

Table 1. Main particulars of candidate ships

	L_{pp} [m]	B_{WL} [m]	T [m]	C_B [-]	x_G [m]	S_w [m ²]
DTC	360	51.0	14.0	0.66	-0.56	21560
KCS	230	32.2	10.0	0.64	-2.18	8992
KVLCC2	320	58.0	20.8	0.81	11.14	27194

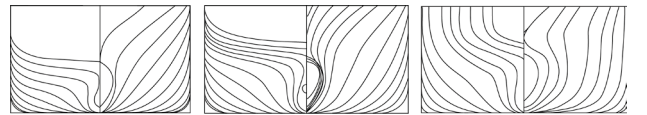


Figure 2. Lines plans of candidate ships DTC, KCS and KVLCC2 (from left to right; not drawn to scale).

4 NUMERICAL METHODS

The aim of the study was to assess the reliability of RANS-based methods for resistance and squat prediction in shallow water and involved sensitivities to turbulence modelling, near-wall treatment and boundary conditions, while a more general interest existed in the performance of BEMs and the computational cost compared to the field methods. While the prediction of pressure-dominated midship sinkage was expected to be accurate with simplified flow models, the problem of accurate resistance prediction –which is itself affected by squat –

was expected to require a fine resolution of near-wall ship flows. Wall functions (WF) are commonly applied in routine computations in industrial applications to economize on computational resources and have been shown to yield good results for resistance prediction in unrestricted waters [5]. However, their application to shallow water ship flows is questionable. Here, computations were performed with both WFs and Low-Reynolds number (LRN) near-wall treatment, integrating the flow equations down to the wall. A Neumann-type boundary condition is usually applied to the tank bottom, imposing zero face-normal velocity (slip wall). However, in ship flows with small UKC a boundary layer may develop and inflicting zero face-tangential velocity (no-slip wall) would yield the physically consistent boundary condition. Field methods draw upon the numerical solution of the Navier-Stokes equations. General mass and momentum conservation equations are formulated in integral notation

$$\frac{\partial}{\partial t} \int_V \rho dV + \int_S \rho \mathbf{v} dS = 0 \quad (1)$$

$$\frac{\partial}{\partial t} \int_V \rho \mathbf{v} dV + \int_S \rho (\mathbf{v} \mathbf{v}) \cdot \mathbf{n} dS = \int_S \mathbf{T} \cdot \mathbf{n} dS + \int_V \rho \mathbf{b} dV \quad (2)$$

where \mathbf{v} denotes the fluid velocity vector, \mathbf{n} is the normal vector of S , which represents the area of the surface of control volume (CV) V , \mathbf{T} denotes the stress tensor and \mathbf{b} a vector representing a force per unit mass. The transport of turbulent momentum is considered by introducing time averaging and fluctuating terms of the flow quantities to the equations, with yet to be introduced approximations for the resulting stress tensor. Forces acting upon the ship hull are obtained by integrating the pressure and shear stresses over the ship's surface allowing for a separate analysis of pressure and friction resistance.

4.1 RANS-METHOD A

Method A refers to the ISIS-CFD solver [6], developed at ECN and available as part of the FINE™-Marine computing suite [7]. The solver is based on the Finite Volume (FV) method to constitute the spatial discretization of the transport equations. Grids can be completely unstructured, and CVs with an arbitrary number of arbitrarily-shaped faces are accepted. Pressure-velocity coupling relies on Rhie and Chow Semi-Implicit Method for Pressure-Linked Equations (SIMPLE) [8]. Free surface flow is modelled with the Volume of Fluid (VoF) approach. The two-equation $k\omega$ -SST model and the two-equation Explicit Algebraic Stress Model (EASM) were applied in the present study for turbulence modelling [9]. Near-wall CV composition was chosen in accordance with the targeted nondimensional wall distance $y^+ = u^* y / v$, where $u^* = \sqrt{\tau / \rho}$ with wall shear stress τ and the distance from the wall to the first interpolation grid point y . Kinematic viscosity is v . In case of application of the LRN approach, y^+ was targeted equal to or less than one. In case of applying

WFs, y^+ was targeted to be ten or greater. The technique included for the modelling of rigid body motions in six degrees of freedom followed the descriptions by [10]. Time-integration of Newton's law for ship motions was combined with analytical weighted or elastic analogy grid deformation to adapt the computational mesh. A parallelized, anisotropic and automatic grid refinement algorithm with dynamic load balancing was implemented and controlled by flow-related criteria. The height of the computational domain was about $0.5L_{pp}$, extended $1.6L_{pp}$ in upstream direction and $2.2L_{pp}$ in downstream direction of the hull. The mesh was generated with the unstructured hexahedral mesh generator Hexpress™ [11]. Prismatic layers were built around the ship hull boundary. A far field boundary condition was applied at the inlet and outlet boundaries. A slip wall condition was applied to the side wall. A pressure boundary condition was applied to the top boundary. Due to port-starboard symmetry of the bare hull ship models, the question arose whether only half of the fluid domain could be modelled and a Neumann boundary condition in the plane of symmetry could map the solution onto the domain image. From a theoretical standpoint, possible occurrence of flow separation, vortex shedding and associated asymmetries in the shallow water ship flow would make modelling of the entire domain mandatory. An associated sensitivity study in preparation of the application of method A showed negligible effects on predictions of resistance and squat and thereafter, advantage was taken in the application of method A of the mentioned symmetry boundary condition.

4.2 RANS-METHOD B

Method B refers to the application of the commercial solver STARCCM+ [12]. The flow equations are discretized using the FV-method. Here, hexahedral control volumes were arranged in an unstructured fashion. The discretization scheme was of second order using central differences. On the surface of the ship prismatic cells were used. A SIMPLE algorithm [13] was used for segregated solution of the velocity-pressure coupling problem. The free surface was modelled using VoF-method and a High-Resolution Interface Capturing (HRIC) scheme to achieve tracking of sharp interfaces between water and air [14]. The applied turbulence model was $k\omega$ -SST [15]. Near-wall grid resolution depended on the wall treatment approach and targeted y^+ . One ship length upstream from the bow a velocity inlet boundary condition was set, specifying flow velocity, turbulent kinetic energy and dissipation rate. An outlet boundary condition was set two to four ship lengths downstream, where the pressure is given directly, a zero-gradient condition is fulfilled and velocities are found from the arithmetic average of neighboring cells. Inflow on these types of boundaries can be considered in terms of the normal component of boundary recirculation. The width of the numerical tank equaled the width of the tank from the model test facilities for the respective test case, i.e. no symmetry condition was

applied in the midship plane. Free-slip conditions were chosen for the tank side walls, specifying zero face-normal velocity components. Bottom cells were assigned the velocity of the undisturbed flow in the no-slip setup. The numerical grid was locally refined in the UKC region, in the stern region and around the free water surface according to the HRIC scheme. Near the outlet boundary the grid was coarsened to provide damping of the downstream propagating ship waves. The domain extended about half a ship length into the air-phase above the ship. Compared to deep water resistance computations, attention needed to be given to the modelling of relative motions between the ship and the tank restrictions. In unrestricted flow, it is possible to take advantage of moving reference frames and resulting motions of the entire domain according to the coupling of fluid forces from the numerical solution and rigid body equations of motion. This approach involves the additional solution of a space conservation equation, but no deformation of CVs (mesh morphing). In shallow water, application of mesh morphing or overset grids is mandatory to model relative motions between the hull and tank bottom. In method B trim and sinkage were modelled with mesh morphing and two different methods to couple the flow and rigid body equations of motion. The first method is the one of the transient solution of the coupled flow and rigid body equations of motion found from Newton's law, hereafter called free motion approach. The second method uses quasi-steady hydrostatic balancing, where the rigid body is released stepwise based on prescribed increments of sinkage and trim. The methods were studied in terms of performance and accuracy.

4.3 BE-METHOD C

Method C is the Rankine Panel Method GLRankine, developed by GL [16], [17]. GLRankine predicts steady ship flows in potential flow regime using nonlinear boundary conditions. Rankine sources are used to model the ship flow and appropriate boundary conditions are satisfied to define the strengths of the point sources. Following the assumption of inviscid, incompressible and irrotational flow, a velocity potential Φ exists, which has to satisfy the Laplacian (3) in the fluid domain and the boundary conditions on the body wetted boundary and free surface (4), on the channel bottom and walls (5) and on the free surface (6)

$$\Delta\Phi = 0 \quad (3)$$

$$(\nabla\Phi - \mathbf{U}) \cdot \mathbf{n} = 0 \quad (4)$$

$$\nabla\Phi \cdot \mathbf{n} = 0 \quad (5)$$

$$\frac{\zeta}{g} = \mathbf{U}\nabla\Phi - \frac{1}{2}|\nabla\Phi|^2 \quad (6)$$

In (3-6) \mathbf{U} is the ship velocity vector and ζ the free surface elevation. An unstructured triangular grid is used on the submerged ship surface and a block-structured

quadrilateral grid is employed on the free surface. Rankine sources are distributed following the desingularization method. Channel boundaries can be modeled either directly, using triangular panels, or employing image sources for rectangular channel cross sections. The Laplacian is satisfied by the formulation of the potential

$$\Phi(\mathbf{x}) = \sum_{j=1}^n q_j G(\mathbf{x}, \xi_j) \quad (7)$$

where $G(\mathbf{x}, \xi_j)$ is a Rankine source of strength q_j and ξ_j denotes the source location points. Upon the determination of the potential and the pressure at each panel, found from Bernoulli's equation, forces acting on the ship hull are available through integration and used to determine iteratively the dynamic trim and sinkage from hydrostatic balancing. Upon determination of the new ship position and orientation, the dynamic boundary condition is used to find the new free-surface elevation, waterline and grid positions. The numerical algorithm is described in detail in [17].

4.4 BE-METHOD D

Method D refers to ShallowFlow, a code for predicting ship squat, developed at the Centre for Marine Science and Technology (CMST) at Curtin University. It is based on slender-body shallow theory [18], [19]. The method uses linearized hull and free-surface boundary conditions. A ship moving in a shallow rectangular canal is modelled as a line of sources and sinks, where the leading-order disturbance velocity potential valid for a ship-fixed coordinate system follows from

$$(1 - F_{nh}^2) \frac{\partial^2 \Phi}{\partial x^2} + \frac{\partial^2 \Phi}{\partial y^2} = 0 \quad (8)$$

subject to the inner boundary condition

$$\frac{\partial \Phi}{\partial y} = \pm \frac{U}{2h} S'(x) \text{ on } y=0_{\pm} \quad (9)$$

and the far-field conditions that $\frac{\partial \Phi}{\partial x}$ and $\frac{\partial \Phi}{\partial y}$ vanish sufficiently far from the ship ($y \rightarrow \pm\infty$), where $S'(x)$ is derivative of the hull cross-sectional area with respect to x . Here, the shallow-water equations are solved by Fourier-transform of (8) subject to (9), whereupon the following expression for the pressure is obtained

$$p(x, y) = -\frac{\rho U^2}{4\pi h \sqrt{1-F_{nh}^2}} \int_{-\infty}^{\infty} iS'(k) \frac{\cosh(\sqrt{1-F_{nh}^2}k[y-0.5w])}{\sinh(0.5\sqrt{1-F_{nh}^2}kw)} e^{-ikx} dk \quad (10)$$

where w is the width of the canal. The so-determined potential is used to find the hydrodynamic pressure and compute the vertical force and trim moment hydrostatically. The method is described in detail in [20].

5 VALIDATION STUDY

Uncertainty analysis of results generated by RANS-methods followed the ITTC recommendation [21]. Resistance, sinkage and trim were determined on grids of various resolutions to investigate the sensitivity of the solution to spatial discretization. The error ratio $E\% = 100(D - S)/D$ compares the experimental data D to the simulation result S . Where applicable, order of discretization error p was determined.

Table 2. Overview of simulation cases for DTC

Setup	WF-SLIP	LRN-SLIP	LRN-WF
Hull	WF	No-slip	No-slip
Bottom	Slip	Slip	WF
CVs	$1.5 \cdot 10^6$	$3.09 \cdot 10^6$	$3.05 \cdot 10^6$

WF: wall function; SLIP: slip wall BC; LRN: Low-Reynolds number approach

Table 3. Grid sensitivity study, DTC simulations with RANS-A WF-WF $k\omega$ -SST

	R _T [N]	z [mm]	9 [1/60°]
Experiment	29.39	11.800	-0.600
$0.86 \cdot 10^6$ CVs	27.04	13.815	0.792
$1.77 \cdot 10^6$ CVs	26.92	13.796	0.756
$3.20 \cdot 10^6$ CVs	27.00	13.787	0.732
Extrapolation	-	13.771	0.708*
Order	-	1.9	0.32

* Second-order assumed

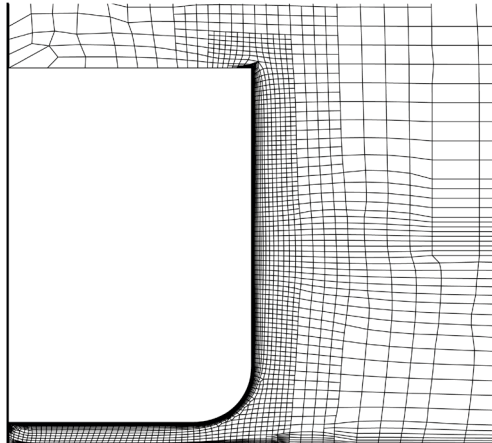


Figure 3. Typical mesh composition at midship section (KCS) in the LRN-WF setup, generated with method A

5.1 DTC

Simulations of the DTC model tests were performed with RANS-method A as a submission of ECN to the PreSquat workshop. Results for application of BE-method D for the DTC were reproduced from the PreSquat workshop, while computations with method C were performed in the framework of this paper. A detailed validation study of both methods with a focus on different container ship shapes is given in [22].

Consistent with the strategy of investigation, Table 2 summarizes the simulation setups with the different near-wall treatments under scrutiny. Figure 3 shows a typical grid composition in the LRN-WF setup at the midship section. A typical computation with $3 \cdot 10^6$ CVs using 24 cores of Intel E5472 processors took about one day of physical time. A grid dependency study was performed at $U=0.791$ m/s ($k\omega$ -SST model) and is summarized in Table 3. Resistance did not show monotonic convergence, but the difference between results was small. Monotonic convergence was observed for sinkage with almost second-order discretization error. Estimated uncertainty for sinkage was $0.2p$. The observed order of convergence for the trim angle was too small ($p=0.32$) for extrapolation and was therefore carried out with assumed second order. Reliable uncertainty estimation as suggested by [21] is generally difficult, but from experience results are believed to be within 10% confidentiality. All remaining computations with method A were performed with the medium grid density. Figure 4 shows the comparison of experimental and computational results with respect to Table 2. Deviations in resistance prediction were observed for the WF-SLIP setup. Results were under-estimated by about 3-5%. Divergence at the two highest speeds occurred due to severe grid deformation as a consequence of unsuitable mesh composition. Applying WFs instead of a slip boundary condition at the bottom wall lead to a further improvement of results in terms of an increase in resistance by about 1-2%, except for the case with the lowest speed. Finally, turbulence modelling was crucial. The predicted resistance with the EASM model was about 3-5% higher than with the $k\omega$ -SST model and in better agreement with experimental results. The effect was more dominant in the lower speed regime. The maximum difference between the limiting cases of applying the $k\omega$ -SST model with WF-SLIP setup and EASM model with LRN-WF setup was 8.3%, valid for $U=0.632$ m/s. However, at the highest speed the LRN-WF setup and computation with the EASM model yielded still more than 5% difference to the experimental result. Sensitivity to turbulence modelling and tendency for under-prediction of resistance is likely to rest with occurrence of flow separation in the aft ship. RANS-based field methods are known to fail in resolving such flow phenomena with required accuracy. Validation with experimental data is required for extended assessment of the accuracy of both turbulence models employed in the present study. Table 4 provides the predicted friction resistance available from the ITTC 57 [23] formula and computations with the EASM model.

Friction resistance prediction was less sensitive to different near-wall treatment and to turbulence modelling. Hence, only results from LRN-WF/EASM cases are presented. Over the entire speed range friction resistance was about 20% higher than the ITTC 57 formula, challenging straightforward application of the friction correlation line for extrapolation procedures in shallow water.

Table 4. Predicted friction resistance for DTC by method A and ITTC 57

U [m/s]	R_F (ITTC) [N]	R_F (RANS-A) [N]	$E\%$
0.475	5.35	6.35	-18.69
0.632	8.98	11.06	-23.16
0.791	13.51	16.62	-23.02
0.949	18.82	23.07	-22.58
1.027	21.74	26.15	-20.29

Unlike for resistance, sinkage (Figure 5) was not observed to be sensitive to different near-wall treatment or to turbulence modelling. In the lower speed range RANS-method A showed over-prediction of sinkage compared to experiments and BE-method D, while for higher speeds agreement becomes fairly good. Both BEMs showed increasing deviations to experimental results with increasing speed. Better performance was observed for nonlinear method C compared to slender-body theory method D. A typical computational setup for the Rankine Panel method C comprised between $1.0 \cdot 10^4$ and $1.8 \cdot 10^4$ panels. Computations were performed on an ordinary desktop PC (2.4GHz, 4GB RAM) and took between one and four hours, depending on the Froude depth number and convergence criteria. With similar computational resources results from method D are readily available within minutes. The case with the lowest speed was not run with method C due to divergence in the overall computational setup. Treatment of low forward speeds requires small panel sizes and high computational effort. These challenges could be circumvented with double-body simulations, which were omitted here. In the lower speed regime, slender-body theory (method D) with linearized hull and free-surface conditions yield good agreement with experiments and the Rankine Panel method C using nonlinear boundary conditions. As F_{nh} increases above 0.6, method D significantly under-predicted the sinkage. This was referred to the increasing importance of nonlinear effects at all speeds in narrow canals, or at high speed in wide canals. Predicted trim angles (Figure 5) were very small (less than one arc minute), which has to be taken into account in the discussion of relative comparison errors. These observations were consistent with the established notion that sinkage is dominating in the subcritical speed regime $U < \sqrt{gh}$, i.e. midship sinkage is an order of magnitude greater than the difference between sinkage at the fore and aft perpendicular. The trend of the experimentally determined trim angle does not correspond to the anticipated quadratic dependence on forward speed. Both BEMs predicted a strong bow-down trim increasing with increasing forward speed.

5.2 KCS

Further investigations were conducted with KCS at $h/T=1.2$ and $h/T=1.3$. Results for KCS and method C for the case at $h/T=1.3$ were taken from a previous study [24].

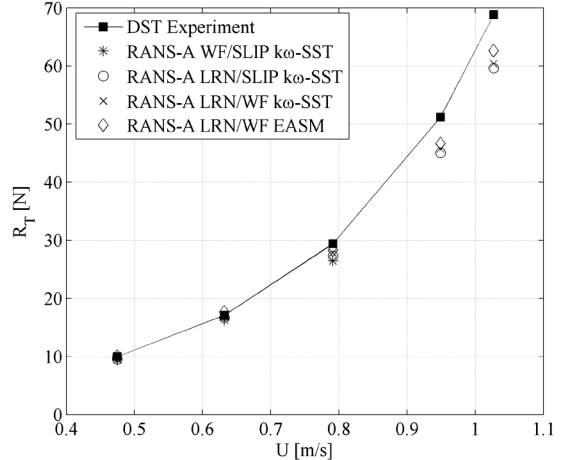


Figure 4. Overview of resistance for DTC predictions in comparison of RANS-method A and DST experiment

Method A is applied in the LRN-WF/EASM setup using medium resolution grids similar to the DTC cases. Results for method B and $h/T=1.3$ are reproduced from [24]. Here, a WF-SLIP setup was applied in good agreement with experimental results in terms of resistance and sinkage. Hydrostatic computations in preparation of RANS-method A gave a different x_G for the static zero trim floating condition than available from the model test (0.04014m instead of 0.0545m). This adjustment was found to have little effect on resistance and sinkage, but improved the observed agreement in trim with experiments and RANS-method A. In the new computational setup, the tank bottom was modelled as a moving no-slip wall according to descriptions in 4.2. A grid sensitivity study led to the choice of a similar medium grid resolution ($4.4 \cdot 10^6$ CVs). Computations were carried out with the actual free motion approach and the iterative hydrostatic balancing routine. The quasi-steady approach was found to be six times faster than the transient resolution of the fluid-body coupling problem. Results differed by less than 2%. In a High Performance Computing (HPC) environment with 64 cores a computation using hydrostatic balancing took between six and eight hours until a converged trend of resistance, trim and sinkage was observed. The efficient application of this approach required careful choice of sinkage and trim increments and relaxation parameters. The stepwise hydrostatic balancing mitigates the well-known shock effect - i.e. divergence of the numerical solution due to severe rigid body motions in the initializing process of the solution - but is only suitable for steady or weakly unsteady flow problems. Resistance predictions for KCS at both water depths are depicted in Figure 6. For the case at $h/T=1.3$ both RANS-methods performed similar and yield fairly good agreement with model experiments. Consistent with the findings of the previous section, resistance prediction with method A in the LRN-WF/EASM approach yield slightly better results compared to the WF-WF/ $k\omega$ -SST setup of method

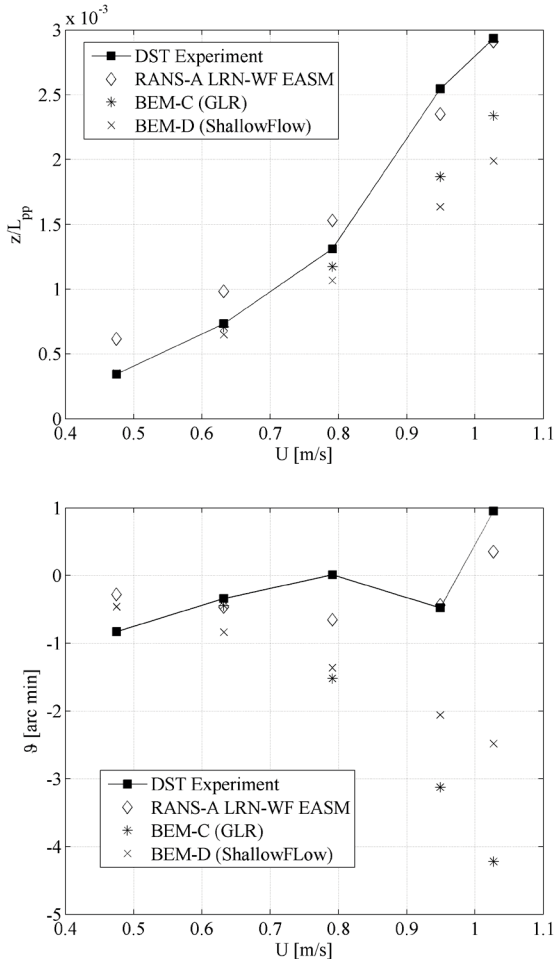


Figure 5. Overview of squat predictions for DTC in comparison of RANS-method A, BEMs and DST experiment

B. The case at $U=0.98$ m/s laid slightly outside this trend. Observed deviations between computations and experiments on one hand, and between different computational setups on other hand were generally smaller in the case study at $h/T=1.3$ compared to $h/T=1.2$. In light of reduced UKC and the experience gained in previous investigations, no effort was made to generate computational setups other than LRN-WF for the case at $h/T=1.2$. Within the present study, grids generated with RANS-method A and B following LRN setups feature 50% to 100% more CVs than grids for WF cases. A grid sensitivity study for method B is presented in Table 5. For resistance and sinkage the difference between computed results from different grids is very small, but did not show monotonic convergence. The trim angle predicted with the finest grid was more than twice the value of the other computations, but generally still small. No attempt was made to perform Richardson extrapolation and discretization error. Remaining computations were performed on the medium size grid. Resistance predictions from RANS-methods and experiments agreed well at lower forward speeds and gave larger deviations as forward speed increased. At the highest speed deviations between RANS-A and experiment on one hand, and RANS-A (EASM) and

RANS-B ($k\omega$ -SST) on other hand were larger than in the DTC study. Findings for both sinkage and trim predictions (Figure 7) were reencountered for the KCS test cases. RANS-methods gave a bow-down trim close to experimental predictions, except for method B at the two lowest forward speeds. BEMs under-predicted sinkage and over-predicted trim in the higher forward speed regime. The Rankine Panel method C was again seen to be closer to model test results at $F_{nh}>0.6$. The overall more bow-down trim predictions of BEMs encountered in investigations with DTC and KCS were referred to the neglect of viscous boundary layer thickening towards the stern. Hull pressure is characterized by deep low-pressure regions at the forward and aft shoulders. If the centroid of this vertical force is ahead of the longitudinal center of floating position, the ship will trim bow-down, and vice versa. Dynamic trim is governed by the difference between large quantities, the downward force at the forward and aft shoulder, and the upward force at the bow and stern. Small changes in hull shape, or submerged volume, will change the balance between each of these, which is discussed for squat of various container shapes in [22]. In light of higher Reynolds-numbers in full-scale ship flows BEMs are expected to show improved agreement when compared to full-scale measurements. For model scale ship flows, systematic studies in conjunction with experience in running the method might be translated into empirical corrections for sinkage and trim, as demonstrated in [22].

Table 5. Grid sensitivity study, KCS simulations with RANS-B LRN-WF $k\omega$ -SST, $h/T=1.2$, $U=0.82$ m/s

	R_T [N]	z [mm]	θ [1/60°]
Experiment	12.53	10.96	-1.429
$4.4 \cdot 10^6$ CVs	10.22	10.38	-1.175
$6.9 \cdot 10^6$ CVs	10.13	10.10	-1.488
$12.5 \cdot 10^6$ CVs	10.23	10.30	-1.191
Extrap.	-	-	-
Order	-	-	-

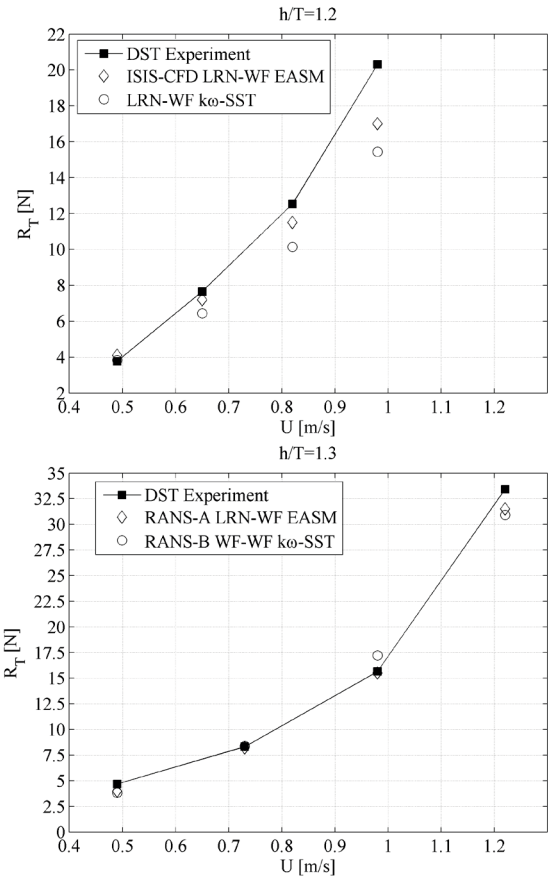


Figure 6. Overview of resistance predictions in comparison of RANS-methods and DST experiments, KCS at $h/T=1.3$ and 1.2

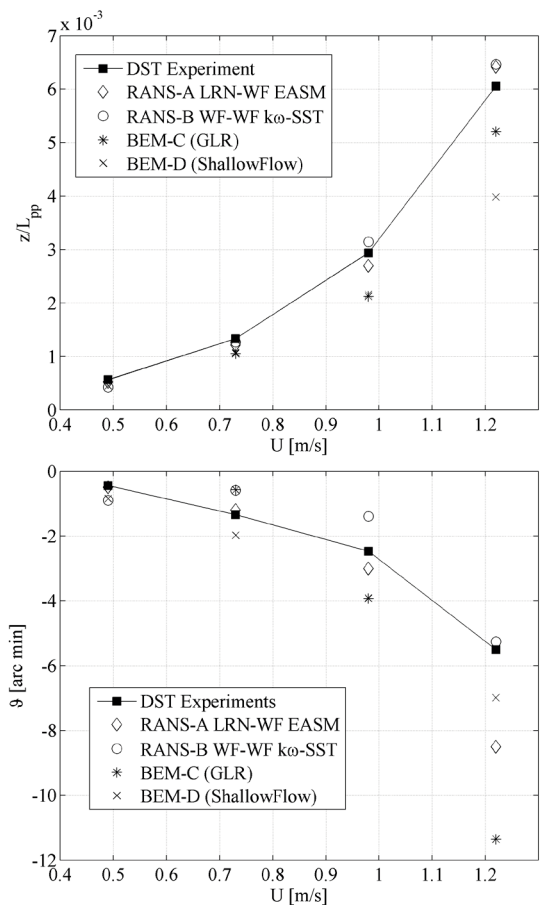


Figure 7. Overview of squat predictions for KCS in comparison of numerical methods and DST experiment, $h/T=1.3$

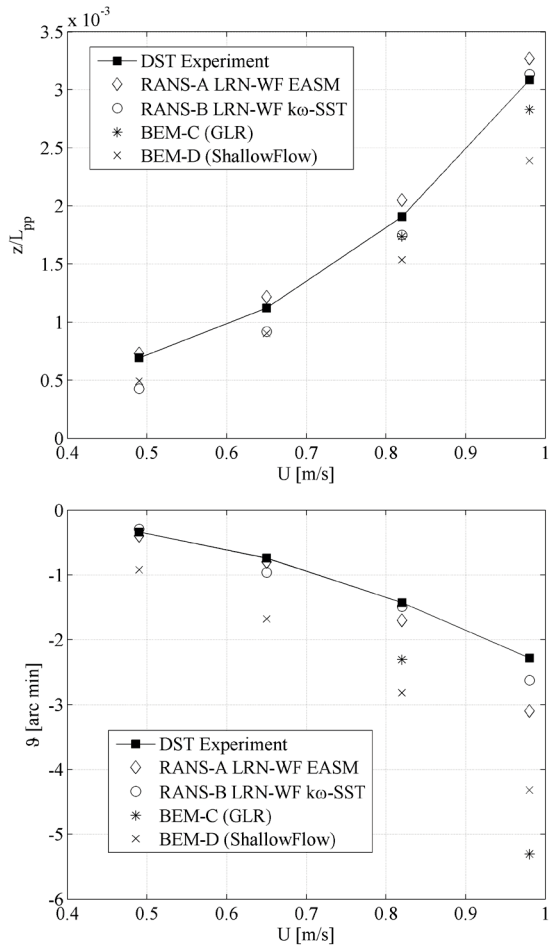


Figure 8. Overview of squat predictions for KCS in comparison of numerical methods and DST experiment, $h/T = 1.2$

5.3 KVLCC2

Numerical methods were applied to simulate the BSHC model tests with KVLCC2, which represented a different kind of ship model compared to the container ships. It was towed in an overall lower Froude depth number range. Resistance predictions by RANS-methods A and B were in good agreement with experimental results in the entire speed range (Figure 9), owing to the generally lower Froude depth number regime compared to the investigations with the containerships. All methods predicted a similar trend bow-down trim, but with deviations between 20-50% in magnitude, where the relative comparison error is larger at low forward speeds. Significant deviations between RANS-methods and BEMs at the highest forward speed were observed for midship sinkage predictions (Figure 10). Moreover, an offset between all computational and experimental results was observed over the entire speed range.

6 INFLUENCE OF SQUAT IN LIFTING FLOWS

Finally, KCS was investigated at $h/T=1.3$ ($U=0.98$ m/s) at three different drift angles with RANS-method B using

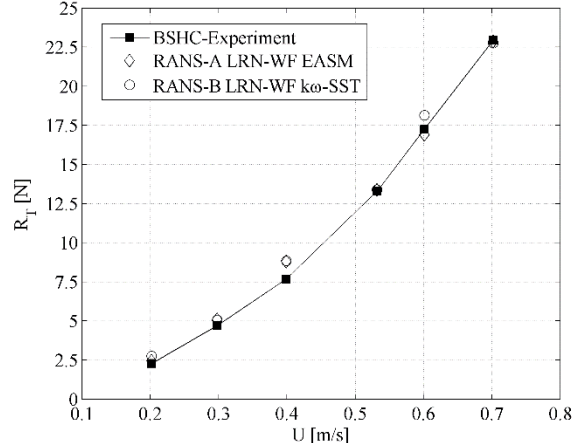


Figure 9. Overview of resistance predictions for KVLCC2 in comparison of RANS-methods and BSHC experiments, $h/T = 1.2$.

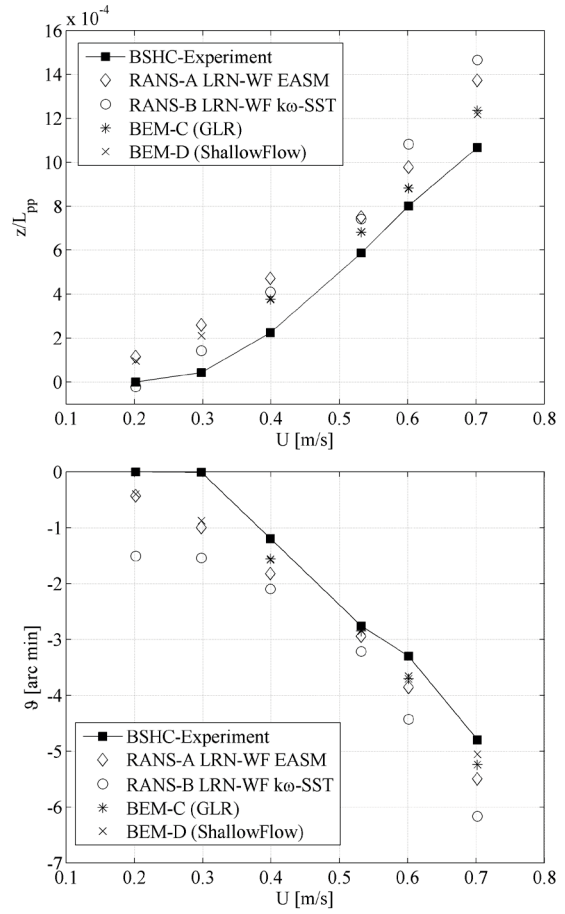


Figure 10. Overview of squat predictions for KVLCC2 in comparison numerical methods and BSHC experiments, $h/T = 1.2$.

the medium size grid. The objective was to assess the influence of squat on hydrodynamic forces X , Y and moment N , valid in a ship-fixed Cartesian coordinate system located at amidships and commonly used in influence of squat on hydrodynamic forces X , Y and moment N , valid in a ship-fixed Cartesian coordinate system located at amidships and commonly used in

maneuvering simulations (x -axis points in the ship's forward direction, y -axis to starboard, z -axis downwards). Two kinds of computations were performed; one with fixed floating position and one with trim and sinkage free using quasi-steady hydrostatic balancing. Roll motion was constrained. Simulated sinkage was close to experimental results, while the bow-down trim was greater by 40%. In general, squat is significantly greater compared to the straight ahead run at the same speed. With the ship drifting at an angle of 12° , sinkage almost doubled, while the bow-down trim became almost five times greater. While the simulation considering squat gave results for Y and N of less than 10% deviation compared to experiments (Table 6), the constrained motion simulation under-predicted Y and N almost by 50%. For the smallest drift angle of 4° deviations were only moderate (Figure 12). Longitudinal force X is 24% higher for the CFD prediction including squat, and 64% higher with the ship being fixed.

Table 6. Comparison of transverse forces and yaw moments for KCS at $\beta=12^\circ$, $U=0.98$ m/s, $h/T=1.3$ between experiment and different computations with RANS-B LRN-WF $k\omega$ -SST

	X [N]	Y [N]	N [Nm]	z [mm]	ϑ [1/60°]
Exp.	-9.88	414.00	726.80	31.17	-15.70
Free	-12.31	443.12	804.82	31.51	-22.19
Fixed	-16.26	227.13	335.53	-	-

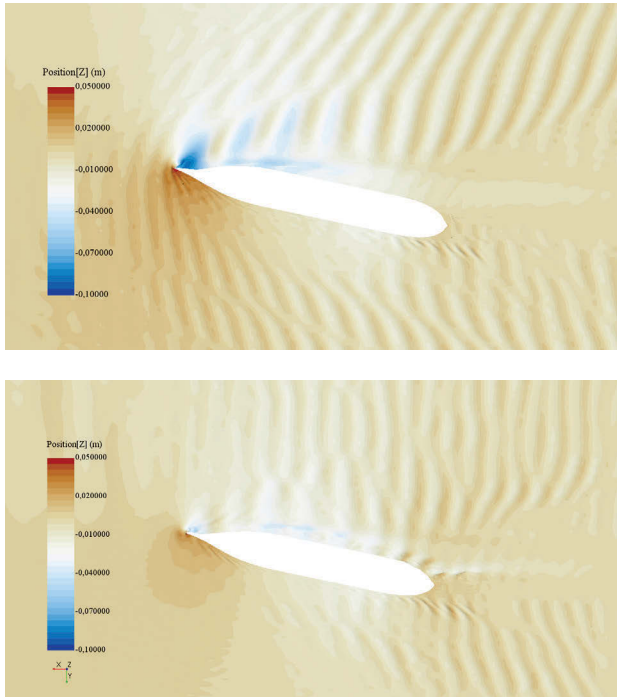


Figure 11. Comparison of free-surface elevation around KCS at $\beta=12^\circ$, $U=0.98$ m/s for simulations with free and fixed sinkage and trim.

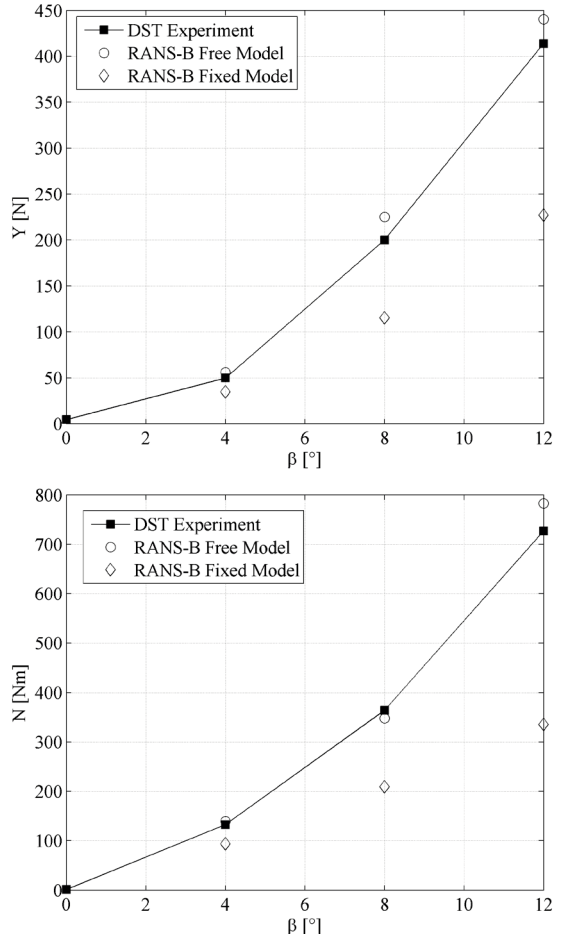


Figure 12. Comparison of transverse forces and yaw moments for KCS at $\beta=12^\circ$, $U=0.98$ m/s between experiment and different computations with RANS-B LRN-WF $k\omega$ -SST

Figure 11 provides insight into the local flow field around the KCS in terms of the free-surface elevation. The massive bow-down trim resulted in a large difference in the water level in the bow area between the wind- and leeward sides. The different water levels induced an increase of transverse force Y - the point of attack in such lifting flows generally lays in the fore ship area - and yaw moment N . In the constrained motion simulation with fixed UKC the difference in water levels is significantly smaller. Such force contributions are anticipated to be proportional to $\rho g \Delta \zeta_l$, integrated over the ship length, where $\Delta \zeta_l$ is the local water level difference. The effect is anticipated to amplify with increasing F_{nh} . In light of the considerable magnification of ship squat in lifting flows, such scenarios should be taken into consideration in UKC management, as the approach of ports might involve maneuvers in which ships might attain drift angles. Besides, results emphasized the requirement of considering squat in shallow water captive maneuvering tests used to derive hydrodynamic coefficients for maneuvering prediction. In this context, the influence of drifting on the roll mode of motion remains to be investigated, as the low-pressure

field along the bilge on the windward side of the ship might induce hydrodynamic roll moments and affect lateral forces.

7 CONCLUSIONS

A validation study on numerical prediction of ship squat and resistance in shallow water was performed with two methods based on the solution of the Reynolds-averaged Navier-Stokes (RANS) equations, a Rankine Panel Method and a method based on slender-body shallow water theory. Validation studies relied on comparison with experimental data for the well-known candidate ships DTC, KCS and KVLCC2 at various water depths, speeds and drift angles. All methods were shown to be capable of predicting midship sinkage with good accuracy at low and moderate forward speeds. BEMs yield larger deviations in higher Froude depth number regimes, especially in predicting trim. Deviations in trim predictions were found to be larger than for midship sinkage. In general, it is desirable to perform repeatability studies in experimental investigations to supplement validation exercises for numerical methods. For BEMs available model test data might serve as a basis for introducing empirical corrections to account for systematic errors in model scale investigations, which are believed to stem from neglecting viscous flow effects. Both BEMs under scrutiny represent a time-efficient tool for squat predictions in shallow water. Viscous flow computations on the basis of the solution of the RANS-equations offer accurate, but expensive squat predictions. For very shallow water ship flows ($h/T < 1.2$), application of simplified models for near-wall treatment at the ship hull and tank bottom results in significant under-prediction of resistance. The EASM turbulence model performed generally better than the $k\omega$ -SST model. At high speeds, where flow separation is likely to be present, resistance in very shallow water condition with such RANS-methods is still under-predicted. In shallow water lifting ship flows, consideration of squat was found to be crucial for accurate computation of transverse forces and yaw moments, which is important for maneuvering predictions.

8 ACKNOWLEDGEMENTS

The authors acknowledge collaboration with model test facilities DST and BSHC in the framework of the PreSquat and SIMMAN workshops. Andreas Gronarz of DST kindly provided model test data for the KCS. Alexander von Graefe and Vladimir Shigunov of DNV GL consulted in running GLRankine. The contribution of Nour Yahfoufi of Université Pierre et Marie Curie to computations related to RANS-method A are acknowledged.

9 REFERENCES

- [1] Mucha, P.; el Moctar, O.; Böttner, C.U. (2014). Technical note: PreSquat - Workshop on Numerical Prediction of Ship Squat in Restricted Waters. *Ship Technology Research - Schiffstechnik*. 61(3): pp. 162-165.
- [2] El Moctar, O.; Shigunov, V.; Zorn, T. (2012). Duisburg Test Case: Post-panamax container ship for benchmarking. *Ship Technology Research - Schiffstechnik*. 59(3), pp. 50-64.
- [3] <http://simman2014.dk/ship-data/>, called 12/10/2015.
- [4] Gronarz, A.; Broß, H.; Mueller-Sampaio; C., Jiang, T., Thill, C. (2009). SIMUBIN - Modellierung und Simulation der realitätsnahen Schiffsbewegungen auf Binnenwasserstraßen (in German). *Report 1939 B*. Development Centre for Ship Technology and Transport Systems (DST).
- [5] Larsson, L.; Stern, F.; Bertram, V. (2003). Benchmarking of Computational Fluid Dynamics for Ship Flows: The Gothenburg 2000 Workshop. *Journal of Ship Research* 47(1): pp. 63-81.
- [6] Queutey, P.; Visonneau, M. (2007). An interface capturing method for free-surface hydrodynamic flows. *Computers and Fluids* 36: pp. 1481–1510.
- [7] Numeca (2015.): *FINETM/Marine User Guide*.
- [8] Rhee C. M.; Chow W. L. (1983). Numerical Study of the Turbulent Flow Past an Airfoil with Trailing Edge Separation. *AIAA Journal* 21(11): pp. 1525-1535.
- [9] Deng, G.B.; Visonneau, M. (2005). Three-dimensional Flow Computation with Reynolds Stress and Algebraic Stress Models. *Engineering Turbulence Modelling and Experiments* 6: pp. 389-398.
- [10] Leroyer, A.; Visonneau, M. (2005). Numerical methods for RANSE simulations of a self-propelled fish-like body. *Journal of Fluids and Structures* 20: pp. 975–991.
- [11] Numeca. (2015.): *HexpressTM User Guide*.
- [12] Cd Adapco. (2015). *STARCCM+-User-Guide 10.06.009*.
- [13] Caretto, L.S.; Gosman, A.D.; Patankar, S.V.; Spalding, D.B. (1972). Two calculation procedures for steady, three-dimensional flows with recirculation. *Proceedings of the 3rd International Conference on Numerical Methods Fluid Dynamics*.
- [14] Ferziger, J.; Peric, M. (1996). *Computational Methods For Fluid Mechanics*. Springer.

- [15] Menter, F.R. (1994). Two-Equation Eddy-Viscosity Turbulence Models for Engineering Applications. *AIAA Journal* 32(8): pp. 1598-1605.
- [16] Söding, H.; von Graefe, A.; el Moctar, O.; Shigunov, V. (2012). Rankine source method for seakeeping predictions. *Proceedings of the 31st International Conference on Ocean, Offshore and Arctic Engineering*, OMAE2012-83450.
- [17] Von Graefe, A. (2015). *A Rankine source method for ship-ship interaction and shallow water problems*. Ph.D. Thesis, University of Duisburg-Essen.
- [18] Tuck, E.O. (1966). Shallow water flows past slender bodies. *Journal of Fluid Mechanics* 26: pp. 81-95.
- [19] Tuck, E.O. (1967). Sinkage and trim in shallow water of finite width. *Schiffstechnik* 14: pp. 92-94.
- [20] Gourlay, T.P. (2014). ShallowFlow: A Program to Model Ship Hydrodynamics in Shallow Water. *Proceedings of the ASME 33rd International Conference on Ocean, Offshore and Arctic Engineering*, OMAE2014-23291.
- [21] ITTC (2008). *Recommended Guidelines and Procedures 7.5-03-01-01: Uncertainty Analysis in CFD Verification and Validation Methodology and Procedures*. <http://ittc.info>, called 12/10/2015.
- [22] Gourlay, T.; Jeong, H.H.; Mucha, P.; Uliczka, K. (2015). Sinkage and Trim of Modern Container Ships in Shallow Water. *Proceedings of the Australasian Coasts and Ports Conference*, Auckland, New Zealand.
- [23] ITTC (2011). *Recommended Guidelines and Procedures 7.5-02-02-01: Resistance Tests*. <http://ittc.info>, called 12/10/2015.
- [24] Mucha, P.; el Moctar, O. (2014). Numerical Prediction of Resistance and Squat for a Containership in Shallow Water. *Proceedings of the 17th Numerical Towing Tank Symposium*, Marstrand, Sweden.

10 AUTHORS' BIOGRAPHIES

Philipp Mucha is a doctoral student and research assistant at the University of Duisburg-Essen (UDE) and Federal Waterways Engineering and Research Institute (BAW) in Germany. His research deals with ship maneuvering in restricted waters and application of numerical methods in ship hydrodynamics.

Ganbo Deng is a Senior Research Fellow at LHEEA (Hydrodynamics, Energetics, Atmospheric Environment) laboratory, École Centrale de Nantes, France. He works on software development for RANSE solvers with the finite volume approach for marine applications.

Tim Gourlay is a Senior Research Fellow at the Centre for Marine Science and Technology (CMST), Curtin University. He undertakes research and consulting work in ship under-keel clearance for ports in Australia and internationally. This work typically includes theoretical development, software development, UKC management guidelines, port liaison and full-scale validation trials.

Ould el Moctar is Professor for Ship Technology and Hydrodynamics at UDE and Managing Director of the Institute for Ship Technology, Ocean Engineering and Transport Systems (ISMT) at UDE. He heads the board of DST.